Integration of fluid dynamics into activation calculations for fusion

T.A. Berry [*,a], C.R. Nobs [a], A. Dubas [a], R. Worrall [a], T. Eade [a], J. Naish [a], L.W. Packer [a]

United Kingdom Atomic Energy Authority, Culham Centre for Fusion Energy, Culham Science Centre, Abingdon, Oxon OX14 3DB, United Kingdom

ABSTRACT

The accurate modelling of the activation of flowing material in a fusion reactor, such as coolant water or lithium-lead breeder, has important safety and shielding implications. Two codes developed at CCFE which account for neutron flux variation have been investigated for the effects of incorporating computational fluid dynamics (CFD) and benchmarked against experimental data. With the inclusion of CFD, both codes are found to be reasonably accurate and benchmarking discrepancies identified previously for ^{16}N water activation data have been clarified. Precise paths calculated using CFD have been used in flowing lithium-lead activation analysis for the first time, with results suggesting that simplified linear paths may give comparable results to detailed CFD paths, but low-detail CFD paths should be avoided. This work paves the way for an accurate and benchmarked set of fluid activation codes.

1. Introduction

The movement and activation of fluids around coolant and breeding circuits in a fusion reactor are an important radiological consideration because flowing material can carry radioactivity to safety-critical areas [1]. This includes gamma-ray emission from activated fluid and activated corrosion products, and secondary activation resulting from neutron emission, with implications for the safety of maintenance personnel and damage to electrical equipment [2]. It is therefore desirable to perform activation analyses which account for fluid motion in a multi-physics approach. Two codes have been developed by CCFE to more accurately simulate fluid activation:

(i) ActiFlow was developed to calculate the decay heat of lithium-lead in breeder blankets, using FISPACT-II [3] to calculate the activity and decay heat in voxels of a flux mesh tally for multiple isotopes simultaneously. The use of FISPACT-II for material activation means that many reactions can be evaluated, making ActiFlow well-suited to simulating complex and heavy materials. It has not previously been benchmarked for fluid activation.

(ii) GammaFlow uses calculated reaction rates in cells to track the concentration of target isotopes around a system. The code requires knowledge of the nuclear reactions and decay modes to be tracked, and requires defined fluid cells. It is therefore well-suited to simulating activated coolant water circuits where there are few reactions of interest. It has been benchmarked previously [4].

In previous work [4] GammaFlow has been applied to the results of a 2019 ITER experiment at the Frascati Neutron Generator (FNG) investigating water activation phenomena associated with ^{16,17}N production, decay and transport [5]. This analysis used the original fluid activation approach, whereby material is shifted between elements of equal volume without accounting for more detailed fluid behaviour such as mixing or residence time distribution in tanks and pipes. The two water circuits used in the experiment are shown in Fig. 1: circuit #2 included a large-volume water expansion tank (WET) for neutron detection which was not present in circuit #1. For circuit #1, GammaFlow predicted gamma-ray counts in a CsI detector from ^{16}N activation with a good degree of accuracy: C/E = 0.87(11) (where C/E is the ratio of calculated to experimental result). For circuit #2, in which complex fluid behaviour would be more significant, the predictions were less accurate, with C/E values approaching 0.5 at low flow rates.

In recent work published by F4E [6], the equations for radionuclide concentration have been adapted to account for WET residence time distributions in the same FNG experiments, calculated using computational fluid dynamics (CFD). The resulting correction factors significantly reduce the discrepancy between modelling and experimental observation, particularly at low flow rates. This suggests that the WET was the main source of the previous inaccuracy, and showed that including CFD in activation calculations is achievable for simple models and can make a significant difference to these C/E results.

For the current work the two CCFE fluid activation codes have been developed to include fluid dynamics and explore their capabilities,
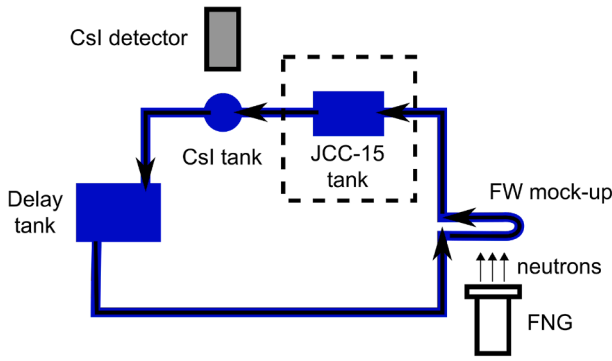
Fig. 1. Schematic of the FNG water activation circuit [5], with arrows showing water flow. Circuit #1 excluded the JCC-15 tank. Circuit #2 included all tanks as shown.

representing a first combination of these codes with CFD calculations. The FNG benchmarking analysis is continued, with effort focused on determining the source of outstanding discrepancies and achieving a first benchmark for ActiFlow. Finally, activation analysis is performed for flowing lithium-lead in a water-cooled lithium-lead (WCLL) breeder blanket test case, using material flow paths determined using CFD and comparing with simplified approaches.

2. Fluid scenarios

Two fluid scenarios water and lithium-lead have been evaluated in this work. These are described in the following subsections.

2.1. Water activation experiments

Coolant water in future tokamaks including ITER will be activated by fusion neutrons. The most active nuclides are produced in (n,p) reactions on ^{16,17}O isotopes [7,8]. The reaction on ^{16}O produces ^{16}N. This decays via beta decay, with a half-life of 7.13 s, and subsequent gamma-ray emission occurs at energies of 6.13 MeV (I=67%) and 7.12 MeV (I=5%) [9]. This will generate increased activity outside the biological shield and is important for safety, for heating in cryogenic systems and for dose to electronics. The reaction on ^{17}O leads to neutron and gamma-ray emission which at the ITER scale could be enough to cause non-negligible secondary activation of pipes and equipment [7,8]. In the present work only the reaction on ^{16}O is evaluated, so all results are given in terms of measured and calculated gamma-ray detection rates.

$$^{16}\text{O}(n,p)^{16}\text{N} \rightarrow {}^{16}\text{N}(\beta(7.13 \text{ s})) \rightarrow {}^{16}\text{O} + \gamma \tag{1}$$
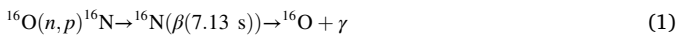
Water in the circuit (Fig. 1) passed through an ITER first-wall (FW) mock-up where it was irradiated by the FNG neutron source. The water then flowed through the neutron detection (JCC-15) WET (circuit #2 only), the gamma-ray detection (CsI) WET, and a delay tank to ensure the decay of all water before returning to the mock-up to complete the circuit.

The experiments were performed for a range of water flow rates, between roughly 10 Lmin^{-1} and 55 Lmin^{-1}, and were repeated for two different distances between the FNG source and mock-up (2 cm and 5 cm). All results in this work use a source separation of 5 cm.

2.2. Flowing lithium-lead breeder material

The tritium breeder blanket is key to achieving the conditions for tritium fuel self-sufficiency in future tokamaks. The WCLL design is one of two European designs being considered for the ITER test blanket modules (TBMs) and the EU-DEMO blanket modules [10]. The molten lithium-lead in the WCLL model cycles through the blanket modules

throughout operation. It therefore experiences a changing neutron flux over time. Understanding the decay heat and activity of the breeder material is important to loss-of-coolant accidents (LOCA), waste disposal and decommissioning. Previous published decay heat analysis has not taken the flowing nature of this material into account [11].

Preliminary blanket calculations in ActiFlow have assumed a single linear path through the lithium-lead manifold, around a breeder zone loop and back through the manifold. For each leg of the circuit, a single lithium-lead flow speed was assumed: 13 mms^{-1} through the manifold; 0.25 mms^{-1} in the feed and return legs of the breeder zone loop; and 0.10 mms^{-1} crossing the front of the breeder zone. However, laminar flow in the channels would be expected to create a distribution in travel times through the high-flux region.

3. Code descriptions and capabilities

3.1. ActiFlow

ActiFlow solves problems using a mesh-based approach. As an input it takes an MCNP [12] output neutron flux mesh file. A mesh-based approach removes the need for an exact definition of the flow volume. ActiFlow takes a user-input coordinate flow path and flow speeds, plotting this path through the neutron flux mesh (or adjacent meshes). The path is split by the voxels it passes through. The time spent in each voxel is summed across i path sections inside the voxel,

$$t = \sum_i \frac{d_i}{v_i} \tag{2}$$

where d_i is the length of path i through the voxel and v_i is the speed. The time spent in a voxel and the flux in that voxel are stored in a list. As well as the user-defined path through the geometry, a zero-flux pseudo-voxel can be added to represent a given fraction of time spent outside the flux mesh. Multiple flow paths can be defined in the same input, in order to simulate splitting and recombination of the flow or distributions in flow speed through the same section of the circuit. These are treated independently by the code, with no in-cycle splitting or mixing, but may be combined in post-analysis.

Using FISPACT-II, the code cycles a unit mass (1 kg) of the user-defined material through the list of voxels consecutively, performing an activation calculation for each and passing the output inventory for a voxel as an input for the next voxel. A full cycle is calculated individually starting and ending on each voxel, to give a final inventory for every voxel in the cycle. To calculate the average decay heat (H, kW/kg) across a circuit, the decay heat in each voxel (h_i, kW/kg) is averaged across the i voxels in the path, weighting by the time t_i spent in each voxel:

$$H = \frac{\sum_i h_i t_i}{\sum_i t_i}. \tag{3}$$

This accounts for variation in flow speed resulting from variation in channel cross-section, and corrects the material volume accordingly. For multiple-path CFD calculations, the same voxel average is made for each path, and then the average of all paths is taken. To calculate the gamma-ray count rate (C, s^{-1}) from water activation, the code uses the average isotope concentrations in the voxels in the detection region alongside calculated efficiencies for the ^{16}N decays [4]:

$$C = \sum_j \sum_i \lambda n_{ij} \frac{R_j V_j}{N_j} \tag{4}$$

where: j are the detection regions; i the voxels within a detection region; λ the constant for the decay; n the concentration of ^{16}N atoms in the voxel (kg^{-1}); R the detector response including branching ratios and efficiency; V the volume of the detection region; and N the number of voxels in the detection region (for averaging). For the experiments described in Section 2.1 the three detection regions were the CsI tank

and its inlet and outlet pipes.

3.2. GammaFlow

GammaFlow uses a cell-based approach, taking calculated neutron reaction rates (here from MCNP) inside fluid cells and using these, along with known decay half-lives, to calculate the rate of decay in given tanks in the circuit.

GammaFlow provides the user with an API with which they can build a model of a circuit. The model may contain cells and circuit components which are joined by pipe elements with specified volumes. The code then moves the material around this circuit in a cycle. The circuit is divided by the code into cells of generally equal volume, simplifying the movement as at each time step, material can be assumed to transfer entirely to the next cell. This also allows for path splitting and in-cycle mixing, as the movement is time-stepped and so the cells are synchronised in time. Where adjacent cells are not of equal volume, a fraction is transferred assuming constant volumetric flow.

After movement, for cells in which reaction rates have been calculated, the corresponding isotopes are added. Then, the decay of the isotopes is computed. So the new isotope count in a given circuit element after time t becomes

$$N(t + \Delta t) = (N(t) + r\Delta t)e^{-\lambda \Delta t} \tag{5}$$

where Δt is the timestep, r is the isotope production rate in the element during irradiation and λ is the decay constant for the decay of the isotope. Note that this is an approximation which is most accurate for small Δt. The activity in an element at time t is equal to $\lambda N(t)$, and this can be converted to a count rate for a particular gamma ray using known branching ratio and efficiency.

4. Calculations and results

4.1. Computational fluid dynamics

Previously, calculations in GammaFlow and ActiFlow have assumed a uniform velocity profile, with residence times in large components proportional to the volume. Due to the flatter profile and mixing through eddy transport, these assumptions hold well for turbulent pipe flow, but in other cases a uniform velocity profile is not appropriate.

In pipes or duct sections where the flow is laminar, faster flow in the middle of the channel leads to a distribution in residence times. One example of laminar flow in a fusion component is a lithium-lead blanket where low rates of flow lead to a sufficiently low Reynolds number for the flow to remain laminar (Re<2000 [13]). Additionally, in expansion tanks turbulence may lead to a spread in residence times. This could include residence tanks in coolant water circuits.

To examine large-volume and complex-shaped components, the residence time was calculated for different flow trajectories using the simpleFoam solver from OpenFOAM 7 [14] for the CsI WET and JCC-15 WET (shown in Fig. 2). The geometries were meshed with snappy-HexMesh to yield an average dimensionless wall distance, y_1^+, of 30 to
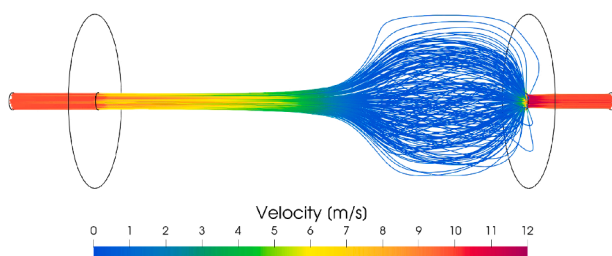

Fig. 2. OpenFOAM-calculated velocity streamlines through JCC-15 WET at a flow rate of 55.1 Lmin^{-1}.

ensure valid use of wall functions with the realisable k-epsilon turbulence model. The total mesh cell counts were 10 million for the CsI expansion tank and 1.1 million for the neutron tank. The residence time calculation was done by solving the steady state flow and measuring the integration times for streamlines from the inlet to the outlet in Paraview. A distribution of residence times was found depending on the seed point and subsequent path of the streamline, which were in general shorter than the residence time calculated based on flow speed and volume. This work shows that there are geometrical fluid dynamics effects in large-volume and complex-shaped components that may need accounting for in a fluid activation code.

4.2. Water activation benchmarking

4.2.1. GammaFlow pipe analysis

The GammaFlow code model of FNG circuit #1 was extended to include a radial velocity profile generated using the OpenFOAM CFD. The CFD model simulated water flow through an approximated FW mock-up and the first part of the pipe (length 17.4 m, diameter 11 mm) leading from the mock-up outlet to the CsI WET. The velocity profile provided pointwise data for the velocity of the water across the diameter of the pipe leaving the mock-up. This allowed the pipe within the GammaFlow model to be split into 20 discrete radial channels, for which no mixing between these channels was assumed.

The results, shown in Fig. 3 and Table 1, suggest that a radial velocity profile in the pipes can have a noticeable effect on measured activity, with greater difference (of up to 9%) observed at lower flow rates where the Reynolds number is lower. This could be relevant to reactor coolant water circuits containing long, thin pipes. The results appear to account for some of the approximate 10% difference between calculation and measurement for this experiment, but not at higher flow rates. Furthermore, any turbulence as would be expected in such a pipe would reduce the size of the correction. The calculation demonstrates that GammaFlow can be used where there are multiple flow speeds along the same path.

4.2.2. ActiFlow analysis

Linear path inputs to ActiFlow were created for both FNG circuit #1 and circuit #2. Flow speeds in each component were calculated using the volume and flow rate. CFD residence times were then calculated for the CsI WET (circuit #1) and the JCC-15 WET (circuit #2) separately, sampling 10^4 flow paths. These residence time distributions were sorted into time bins and each bin was used to define a separate ActiFlow input speed through the component. For comparison, the CFD residence times calculated for the JCC-15 WET in separate work by F4E (ref. [6]) were used to create another set of inputs.

The results were compared with the original (no CFD) GammaFlow results and those measured during the experiment. The gamma-ray emission in ActiFlow was obtained using the number of ^{16}N atoms in the CsI WET, inlet and outlet, as calculated by FISPACT-II, the known half-life, and the detection efficiency of 2.32% in the energy range 5.5–6.5 MeV, calculated previously by MCNP simulation [4]. This is equivalent to the approach used for GammaFlow.

The results of the circuit #1 analysis are shown in Fig. 3 and Table 1. ActiFlow predicts virtually the same count rates as GammaFlow, with an average accuracy of C/E = 0.90(2). The ActiFlow material sees almost identical neutron fluence to that in GammaFlow. The calculation demonstrates that for a basic water circuit ActiFlow and GammaFlow give similar results, here predicting ^{16}N count rates within 2% of each other at all flow speeds.

The remaining 5–15% underestimation is suggested to result from fluid behaviour. Residence times were calculated for the CsI WET for several flow rates, and sorted into 2–10 ms bins to create a new set of inputs. The difference between the ActiFlow results with and without CFD, shown in Fig. 3, is less than 1%, suggesting that the CsI WET is not the dominant source of the underestimation for circuit #1. However,

Table 1
Calculated and measured ^{16}N counts per second (CPS) by flow rate for both FNG water activation circuits, at a source-FW distance of 5 cm.

| Flow rate, L/min	Circuit #1 ^{16}N count rate, CPS					Flow rate, L/min	Circuit #2 ^{16}N count rate, CPS			
	GammaFlow	GammaFlow with pipes CFD	ActiFlow	ActiFlow with CsI tank CFD	Measured		ActiFlow	ActiFlow with WET CFD (CCFE)[a]	ActiFlow with WET CFD (F4E)[b]	Measured
10.3	1824	1985	1852	1869	1993	10.5	424	542	781	852
16.4	1714	1806	1746	1746	1922	16.5	686	934	908	1025
22.0	1519	1585	1548	1550	1697	22.5	773	994	911	1008
27.5	1345	1398	1367	1372	1507	28.6	786	960	870	924
34.4	1167	1208	1186	1190	1344	34.9	757	-	816	917
39.4	1062	1097	1079	1083	1228	41.3	715	935	759	885
44.1	978	1009	996	997	1125	55.0	-	761	653	-
50.1	887	915	904	906	1031	74.0	-	-	542	-
55.1	823	848	839	838	948					

[a] CFD residence times for JCC-15 WET calculated by CCFE.
[b] CFD residence times for JCC-15 WET calculated by F4E in separate work presented in ref. [6].
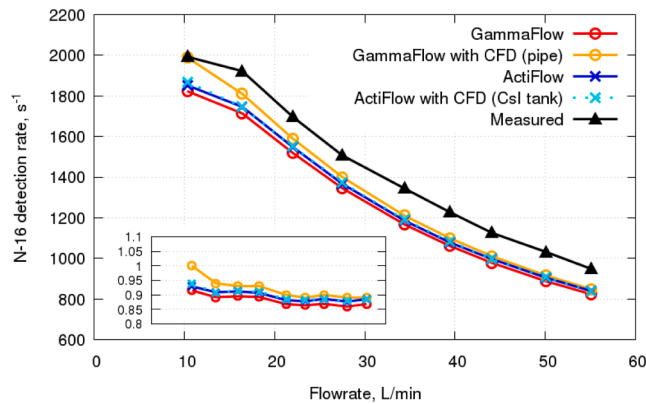
Fig. 3. Measured and calculated ^{16}N activity in CsI tank for FNG circuit #1 using GammaFlow and ActiFlow, with and without fluid dynamics considerations. Inset: C/E values are plotted for calculations.

water flow through the FW mock-up and pipes could explain the difference.

The underestimation is more exaggerated for circuit #2 where, for ActiFlow and GammaFlow without CFD, at low flow rates in particular the C/E values are as low as 0.5 (Fig. 4, Table 1). The flow rate dependence is consistent with the omission of fluid dynamics behaviour in the neutron tank. This is discussed in refs. [4,6]. The results for both circuits demonstrate that ActiFlow and GammaFlow give similar results when CFD is not included.
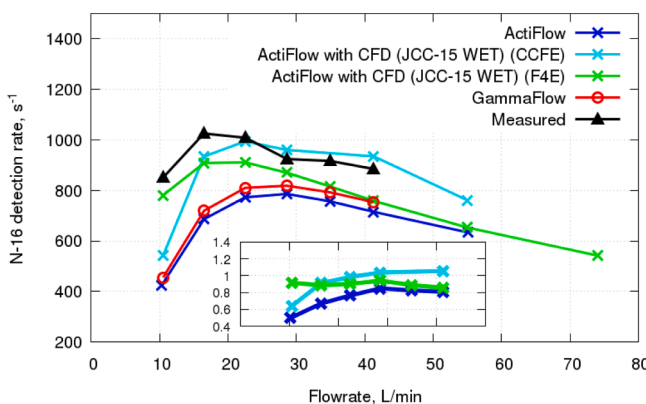

Fig. 4. Measured, ActiFlow (with and without JCC-15 WET CFD residence times) and GammaFlow activity in FNG circuit #2. GammaFlow results are identical to those calculated in ref. [4]. Inset: C/E values for ActiFlow calculations.

The ActiFlow results incorporating CFD in the JCC-15 WET differ depending on the source of the residence times (CCFE vs. F4E). This is despite them simulating the same cylindrical tank geometry. When the residence times calculated by CCFE are used, the underestimation at the lowest flow rate reduces to 36% while at the highest measured flow rate ActiFlow overestimates the count rate by 6%. If instead the residence times calculated by F4E are used, the underestimation at the lowest flow rate is just 8%, and at the highest measured flow rate the underestimation is 14%. We suggest that the inclusion of a longer WET inlet pipe in the F4E simulation increases jetting at low flow rates, leading to higher count rates. A difference of selected turbulence model may account for the difference. Weaker convergence of the CFD residence time distributions in the present work is a further source of uncertainty. This highlights the importance of accurate conditions and the value of comparing simulations.

4.3. ActiFlow calculations with a PbLi test case

A breeder zone test case was devised in order to examine the effect of CFD inclusion for lithium-lead flow (without magnetohydrodynamic effects). This was a single loop through a DEMO WCLL blanket consisting of homogenised layers (mixtures of tungsten, Eurofer, water and lithium-lead). The lithium-lead corresponds to a $Pb_{83}Li_{17}$ mixture containing 17.5% lithium. The loop was in the outboard equatorial plane (Fig. 5), moving from an inlet surface, along a feed channel radially towards the first wall, up and around a buffer plate, and along a return channel to the outlet surface. The model used a simplified Cartesian blanket geometry and a planar source created using the flux in front of the first wall in the DEMO model as described below.

A CFD calculation was performed using liquid lithium-lead, and flow paths and speeds were calculated for tracks beginning on the inlet and ending on the outlet. Between reaching the outlet and re-joining at the inlet, a zero-flux time of 67% of the total cycling time, representing manifold and ex-blanket time, was added. The neutron flux was calculated in MCNP 6.2 with nuclear transport data from JEFF 3.3 [15]. This used the 2017 DEMO baseline MCNP model. The ActiFlow calculation used the 5.2-year DEMO phase 1 (20 displacements per atom (DPA))
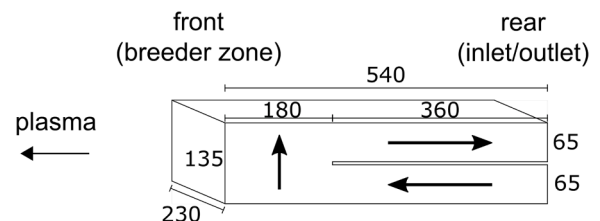
Fig. 5. Dimensions of lithium-lead DEMO WCLL breeder zone test case (mm). Arrows show PbLi flow direction.

irradiation schedule. EAF-2010 [16] was used for activation and decay data. The lithium-lead was cycled in ActiFlow with an averaged flux throughout the schedule and the exact breeder zone path was only used in the final circuit. Five path scenarios were simulated:

(i) a simple non-CFD square loop with path down the centre of channels and speeds as described in Section 2.2;

(ii) identical to (i) but travelling to the front of the breeder zone, representing a conservative case;

(iii) one flow path, using a CFD track beginning in the centre of the inlet surface;

(iv) four flow paths, using CFD tracks beginning at points forming a uniform 2x2 grid on the inlet surface;

(v) 25 flow paths, using CFD tracks beginning at points forming a uniform 5x5 grid on the inlet surface.

The plots in Fig. 6 give an indicator of the flow paths and neutron fluxes in each of the calculations. The post-irradiation decay heat (kW/kg) for each test case was obtained using the path averaging method in Section 3.1. The results are shown in Fig. 7.

The differences in decay heat are greater at short timescales. At shutdown, relative to the result of 1.05×10^{-3} kWkg^{-1} for the simple loop (i) calculation, the conservative loop is 152% hotter, the 1x1 loop is 56% cooler, the 2x2 loop is 28% hotter and the 5x5 loop is 9% cooler. After one year, relative to 2.35×10^{-6} kWkg^{-1} for the simple loop (i), the conservative loop is 69% hotter, the 1x1 loop is 28% cooler, the 2x2 loop is 1% hotter and the 5x5 loop is 11% cooler.

The results indicate that a more detailed description of the flow through the breeder zone has a significant effect on the predicted blanket activation, with the most detailed and physically accurate flow (v) giving less conservative estimates than the simple loop (i). When using CFD, a single streamline (iii) passes tightly around the baffle plate and appears unsuitable to represent the whole flow. Using four streamlines (iv) samples more of the breeder zone but gives higher decay heat estimates than (v), with increased uncertainty owing to the small number of points sampled. A simplified path down the centre of the channel gives results reasonably close to a calculation using a number of streamlines, and so is a fair assumption where complete accuracy is not essential.

5. Discussion and conclusions

Both GammaFlow and ActiFlow have now been compared with experimental water activation results. After accounting for CFD in the JCC-15 WET in ActiFlow calculations for circuit #2, the least accurate result is C/E=0.64 at the lowest flow rate, using the CFD calculations performed in this work. These compare to a minimum value of C/E=0.51 for GammaFlow obtained in previous work [4], showing a clear improvement when fluid dynamics are taken into account. It is possible that accounting for radial velocity distributions in the pipes could provide a further correction at low flow rates only, but further work is needed. The remaining difference is therefore expected to result from residence time distributions inside the FW mock-up component.
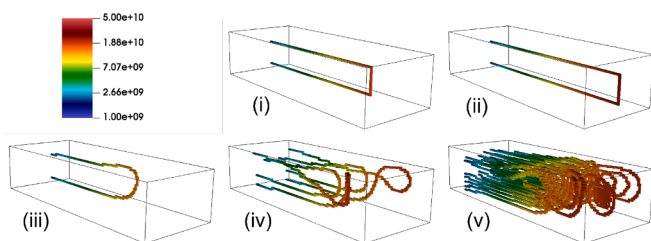

Fig. 6. Neutron fluxes (ncm^{-2}s^{-1}) through voxels of the five different PbLi test case flow scenarios.
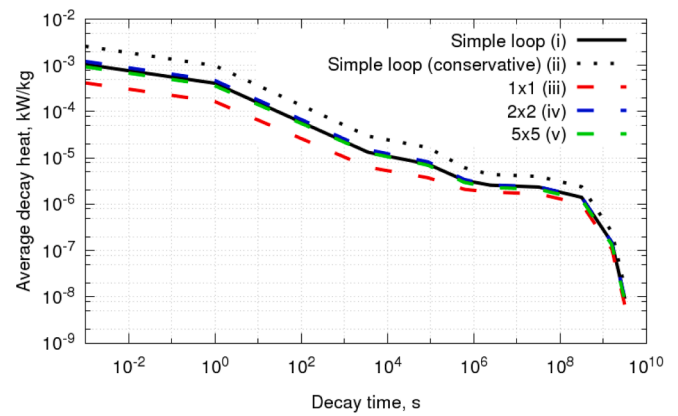

Fig. 7. Decay heat per unit PbLi for different CFD and non-CFD flow path scenarios (described in text) through the breeder zone test case.

Analysis of a simplified lithium-lead breeder zone test case using ActiFlow has shown that there is a large variation in decay heat result depending on the number of paths simulated. The results in Fig. 7 suggest that using few paths or one single path is inaccurate, when compared to the more detailed 5×5 flow (v). Meanwhile, the simple rectangular loop (i) gives decay heat results only around 10% hotter than the detailed flow. From this we suggest that fluid activation calculations using such a loop would give reasonably accurate results. This simplification could increase the computational efficiency of breeder blanket fluid activation calculations accounting for multiple breeder zone loops around the tokamak.

Through this work the strengths and weaknesses of the two codes have been clarified and the impact of considering fluid behaviour in activation calculations has been highlighted. The strengths of the GammaFlow code lie in its ability to accurately model a spatially well-defined flow in a relatively fast calculation time, for simple materials. The code is designed to allow pipe splitting and recombination and implicit mixing, with the eventual aim of modelling the complex networks of water coolant pipes anticipated in future fusion reactors. ActiFlow is versatile in terms of the materials, reactions and paths which it can model. The multiple-flow capability allows the code to account for residence time distributions or path splitting in limited situations. The mesh-based approach is inefficient when simulating well-defined flows such as the FNG water activation circuit, but advantageous where flow geometry is not completely defined. In addition, as demonstrated through the PbLi test case study it allows for more detailed analysis of individual flow paths.

Within a reactor environment, pipe systems can often take the form of lengthy and complex networks including components such as junctions, holding tanks and pumps. Due to the complex nature of these systems, the computational cost of full-system CFD calculations could be prohibitive. One way to overcome this could be to create a repository of common components where each could be modelled using a CFD code, generating a radial velocity profile. Users could then build a model with these parametrised components using the GammaFlow API, allowing fast, standardised calculations which account for fluid dynamics throughout the system.

The two codes have advantages and disadvantages owing to different approaches, and between them cover a range of problems. A combined code would therefore be advantageous, with the possibility of choices between mesh-based and cell-based sampling, the use of known reaction/decay parameters or an activation code, and user-defined cells or parametrised components.

Declaration of Competing Interest

The authors declare that they have no known competing financial

interests or personal relationships that could have appeared to influence the work reported in this paper.

Acknowledgments

References

[1] A. Žohar, L. Snoj, On the dose fields due to activated cooling water in nuclear facilities, Prog. Nucl. Energy 117 (2019) 103042.

[2] I. Palermo, M. García, C. Bachmann, S. Ciattaglia, U. Fischer, C. Gliss, Impact of the flowing activated water on maintenance and electronic functioning for the pre-conceptual design of the European DEMO fusion reactor, Fusion Eng. Des. 153 (2020) 111499.

[3] J.-C. Sublet, J.W. Eastwood, J.G. Morgan, M.R. Gilbert, M. Fleming, W. Arter, FISPACT-II: An Advanced Simulation System for Activation, Transmutation and Material Modelling, Nucl. Data Sheets 139 (2017) 77–137.

[4] C.R. Nobs, J. Naish, L.W. Packer, R. Worrall, M. Angelone, A. Colangeli, S. Loreti, M. Pillon, R. Villari, Computational evaluation of N-16 measurements for a 14 MeV neutron irradiation of an ITER first wall component with water circuit, Fusion Eng. Des. 159 (2020) 111743.

[5] F. Andreoli, M. Angelone, A. Colangeli, U. Besi Vetrella, S. Fiore, D. Flammini, P. Del Prete, S. Loreti, G. Mariano, G. Mazzitelli, F. Moro, G. Pagano, A. Pietropaolo, M. Pillon, N. Terranova, R. Villari, J. Naish, C.R. Nobs, L.W. Packer, Comparison between measurement and calculations for a 14 MeV neutron water activation experiment, EPJ Web Conf. 239 (2020) 21002.

[6] R. Pampin, F. Cau, M. Fabbri, J. Izquierdo, A. Portone, Improving the estimation of activation levels in flowing liquids under irradiation and decay, Nucl. Fusion 61 (2021) 036003.

[7] R.T. Santoro, V. Khripunov, H. Iida, R.R. Parker, Radionuclide production in the ITER water coolant, Proc. Symp. Fusion Eng. 1 (1998) 137–140.

[8] Q. Yang, T. Dang, D. Ying, G. Wang, M. Loughlin, Activation analysis of coolant water in ITER blanket and divertor, Fusion Eng. Des. 87 (2012) 1310–1314.

[9] D.R. Tilley, H.R. Weller, C.M. Cheves, Energy levels of light nuclei A = 16-17, Nucl. Phys. A 564 (1993) 1–183.

[10] J. Aubert, et al., Design and preliminary analyses of the new Water Cooled Lithium Lead TBM for ITER, Fusion Eng. Des. 160 (2020) 111921.

[11] T. Eade, M. Garcia, R. Garcia, F. Ogando, P. Pereslavtsev, J. Sanz, G. Stankunas, A. Travleev, Activation and decay heat analysis of the European DEMO blanket concepts, Fusion Eng. Des. 124 (2017) 1241–1245.

[12] J.T. Goorley, et al., Initial MCNP6 Release Overview - MCNP6 version 1.0. Technical Report, LANL, Los Alamos, 2013.

[13] O. Reynolds, IV. On the dynamical theory of incompressible viscous fluids and the determination of the criterion, Philos. Trans. R. Soc. 186 (1895) 123–164.

[14] H.G. Weller, G. Tabor, H. Jasak, C. Fureby, A tensorial approach to computational continuum mechanics using object-oriented techniques, Comput. Phys. 12 (1998) 620.

[15] A.J.M. Plompen, et al., The joint evaluated fission and fusion nuclear data library, JEFF-3.3, Eur. Phys. J. A 56 (2020) 181.

[16] J.-C. Sublet, L. Packer, J. Kopecky, R. Forrest, A. Koning, D. Rochman, The European Activation File: EAF-2010 neutron-induced cross section library. Technical Report, CCFE-R (10) 05, 2010.